Electronic structure of defects and defect clusters in narrow band-gap semiconductor PbTe

2004 J. Phys.: Condens. Matter 16 S5277

(http://iopscience.iop.org/0953-8984/16/44/024)

INSTITUTE OF PHYSICS PUBLISHING JOURNAL OF PHYSICS: CONDENSED MATTER

J. Phys.: Condens. Matter **16** (2004) S5277–S5288 PII: S0953-8984(04)85452-3

Electronic structure of defects and defect clusters in narrow band-gap semiconductor PbTe

S D Mahanti and D Bilc

Department of Physics and Astronomy, Michigan State University, East Lansing, MI 48824, USA

Received 26 August 2004
Published 22 October 2004
Online at stacks.iop.org/JPhysCM/16/S5277
doi:10.1088/0953-8984/16/44/024

Abstract

Lead chalcogenide salts PbSe and PbTe are IV–VI narrow gap semiconductors whose study over last several decades has been motivated by their importance in infrared detectors, lasers and thermoelectrics. Recently a class of systems, $AgSbPb_{2n-2}Te_n$, has been found to be excellent high temperature thermoelectrics. Since electronic properties of semiconductors in general and thermoelectric behaviour in particular, are dominated by defects, we have carried out *ab initio* electronic structure calculations of Ag and Sb substitutional defects in PbTe. We find that these defects give rise to deep defect states and the electronic structure near the gap depends sensitively on the micro structural arrangements of these defects. The modified electronic structure may be responsible for the observed high temperature thermoelectric properties of the above compounds.

(Some figures in this article are in colour only in the electronic version)

1. Introduction

Narrow band-gap III–V, II–VI and IV–VI semiconductors have been of great interest for the last four decades for their fundamental solid state physics and for their applications in infrared devices and thermoelectric materials. In recent years they have attracted attention for spintronics and high performance thermoelectrics. Some of the examples of these semiconductors are InAs, GaSb, AlSb, InMnSb, GaMnAs for III–V systems, $Hg_{1-x}Cd_xTe$, $Hg_{1-x}Zn_xTe$, $Hg_{1-x}Zn_xSe$ for II–VI systems and $Pb_{1-x}Sn_xTe$, $Ge_{1-x}Mn_xTe$ for IV–VI systems.

Lead chalcogenide salts PbSe and PbTe are IV–VI narrow gap semiconductors whose study over last several decades has been motivated by their importance in infrared detectors, in light-emitting devices, and more recently as infrared lasers in fibre optics, as thermophotovoltaics and thermoelectrics, in solar energy panels, and in window coatings [1–3]. Since our interest is in high performance thermoelectrics operating at high temperatures we will focus on this aspect of PbTe and related systems. In fact PbTe was one of the first materials studied

by Ioffe and his colleagues in the middle of the last century when there was a revival of interest in thermoelectricity [4]. This compound, its alloys with SnTe and PbSe and related compounds called TAGS (alloy of $AgSbTe_2$ and GeTe) were for many years the best thermoelectric materials at temperatures ∼700 K [5]. In recent years quantum wells of $PbTe/Pb_{1-x}Eu_xTe$, $PbSe_{0.98}Te_{0.02}$/PbTe superlattices [6] and novel quaternary compounds [7] $AgSbPb_{2n-2}Te_{2n}$ ($n = 9, 10$) have attracted considerable attention because of their large thermoelectric figure of merit (FOM). Since the thermoelectric performance of a semiconductor depends sensitively on its electronic structure [8, 9], it is important to understand the nature of the electronic states which control the transport processes in these systems.

It is well known that the thermoelectric FOM (ZT where T is the operating temperature of the device) depends on the thermopower (S) through the relation $ZT = \sigma S^2 T/\kappa$, where σ and κ are the electrical and thermal conductivities of the material [10]. Clearly a large ZT requires large values of S at operating temperatures. Since S depends sensitively on the nature of the electronic states near the gap [8, 9] it is important to have a fundamental understanding of the electronic states of PbTe, PbSe and related systems containing defects and defect clusters such as $PbTe/Pb_{1-x}Eu_xTe$, $PbSe_{0.98}Te_{0.02}$/PbTe multi-layers and $AgSbPb_{2n-2}Te_{2n}$ ($n = 9, 10$) compounds. It is believed that the modification of the electronic states near the band gap region of PbTe caused by self-assembled quantum dots acting as zero-dimensional systems embedded in a three-dimensional matrix (in the case of multi-layers) and nanostructures formed by Ag and Sb ions in the PbTe matrix might be responsible for the observed superior thermoelectric properties of these different compounds [6, 7].

Defects (shallow and deep) in semiconductors are known to profoundly alter their electronic structure near the band gap and control their transport properties. Unlike shallow impurity levels, which are produced by the long-range Coulomb potential, deep levels are produced by the short-range atomic-like defect potential [11]. It is believed that shallow impurities primarily control the magnitude and type of conductivity, whereas deep defect levels primarily control the charge-carrier life-time. The detailed understanding of shallow defects in common semiconductors traces back to the classic work of Kohn and Luttinger and can be regarded as basically understood [12, 13]. However the problem of defects in narrow-gap semiconductors, particularly the physics underlying deep defect states, is far from understood. In these systems both shallow defects caused by the long-range Coulombic potential and deep defects formed by short range interactions and mixtures of these may coexist. In this paper we are mainly interested in investigating the nature of electronic states in $AgSbPb_{2n-2}Te_{2n}$ ($n = 9, 10$). Since the precise structural arrangements of Ag and Sb atoms in these compounds are not known from x-ray diffraction measurements [7], we will treat these quaternary compounds as PbTe containing Ag and Sb substitutional defects with different types of structural arrangements and see how these alter the electronic structure of PbTe.

The theory of deep defects in semiconductors in general and narrow band-gap semiconductors in particular has a long history. For substitutional defects in PbTe Lent *et al* [14] presented a simple chemical theory of s- and p-bonded substitutional impurities almost 17 years ago. This theory naturally gave deep defect states near the fundamental band gap and also predicted resonant levels further away from the gap. In this paper we review the basic ideas underlying this theory and discuss the results of our recent attempts to understand the physics behind these deep defect states using *ab initio* electronic structure calculations. We also discuss how these defect states get modified when different types of impurity microstructures are present. Given the close structural relationship of $AgSbPb_{2n-2}Te_{2n}$ to PbTe, a fundamental question is how the PbTe electronic structure gets modified by intensive substitution with Ag and Sb atoms and their micro structural arrangements.

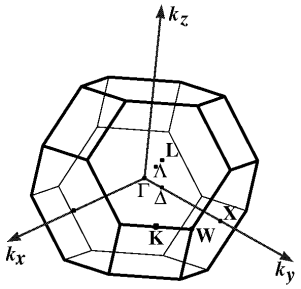

Figure 1. Fcc Brillouin zone of PbTe.

The arrangement of the paper is as follows: in section 2 we discuss briefly the electronic structure of the parent compound PbTe focusing on the gap, bonding and ionicity. In section 3.1 we review the earlier simple chemical theory of Lent *et al* to explain the impurity levels associated with substitutional point defects in PbTe. In section 3.2 we give the results of our *ab initio* electronic structure calculations for defects and defect clusters obtained using different supercell models. Finally in section 4, we summarize our results.

2. Electronic structure of PbTe

The rocksalt-structure semiconductors PbS, PbSe and PbTe show a series of electronic anomalies relative to the usual II–VI semiconductors. For example the direct gap occurs at the L point and the order of the band gap and valence band maximum energies in going from S to Te are anomalous. The band gap pressure coefficient is also anomalous, it is negative. There have been innumerable electronic structure calculations in these compounds [15]. Wei and Zunger [16] have recently carried out extensive electronic structure calculations using the local density approximation (LDA) [17] as implemented by the linearized augmented plane-wave (LAPW) method [18] and have argued that the above anomalous features can be ascribed to the occurrence of the Pb s-band below the top of the valence band, setting up coupling and level repulsion at the L point. Albanesi *et al* [19] calculated the frequency dependent dielectric constant of PbSe and PbTe using the electronic structure (obtained with FLAPW) within both the LDA and the generalized gradient approximation (GGA) [20]. They found a large dielectric constant for PbTe in agreement with experiment. We have carried out all electron FLAPW calculations within both LDA and GGA to confirm the findings of Wei and Zunger and to analyse the covalency between Pb and Te (by calculating the effective ionic charge) and the bonding and antibonding nature of the electronic states near the fundamental gap. We have used the WIEN2K package for our calculations [21]. Scalar relativistic corrections were included and spin–orbit interaction (SOI) was incorporated using a second variational procedure [22].

The fcc Brillouin zone and the band structure of PbTe are given in figures 1 and 2. The band structure results show that PbTe is a direct band gap semiconductor with a small gap value of $\sim$0.09 eV at experimental volume $V_{\rm exp}$. The gap occurs at the L point in the fcc Brillouin zone. Orbital analysis shows that Te and Pb p states hybridize, suggesting covalent interaction between Pb and Te atoms. In order to find the ionicity of Pb and Te atoms we have computed the electronic charge around each atom according to Bader's 'Atoms in Molecules' theory [23]. The results show an ionic state of $Pb^{+0.64}Te^{-0.64}$ which is much smaller than that of the pure ionic model $Pb^{+2}Te^{-2}$. Therefore in PbTe the covalent interactions play an important role. The reduction in formal charges from $2(-2)$ to $0.64(-0.64)$ is consistent

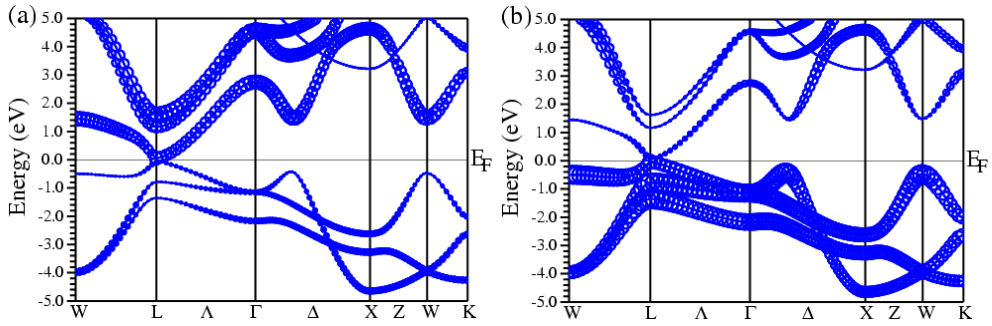

Figure 2. Band structure of PbTe at V_{exp} along different directions in the fcc Brillouin zone. Orbital character of: (a) Pb p and (b) Te p. The size of the circles is proportional to the orbital character.

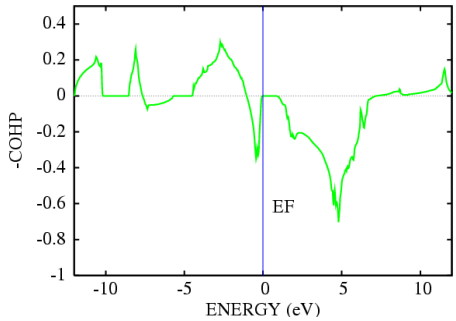

Figure 3. –COHP as a function of energy for PbTe without including spin–orbit interaction (SOI).

with the large dielectric constant of PbTe. We have also performed crystal orbital Hamilton population (COHP) analysis which is a bond-detecting tool for solids and molecules. COHP partitions the band structure energy (in terms of the orbital pair contributions) into bonding, nonbonding and antibonding energy regions within a specified energy range [24]. In figure 3 we plot –COHP as a function of energy. Positive values of –COHP describe bonding energy regions whereas negative values describe antibonding energy regions. As can be seen in figure 3 in the $(-1, 0)$ eV energy range the electrons occupy antibonding states with both the valence band maximum (VBM) and conduction band minimum (CBM) at the L point being antibonding states.

3. Electronic structure of Ag and Sb defects in PbTe

3.1. Impurity levels in PbTe—a simple chemical theory

Lent *et al* presented a simple chemical theory of s- and p-bonded substitutional point defects in PbTe [14]. The central idea of this theory was that due to large static dielectric constant of ($\varepsilon \sim 10^3$) [19], the Coulombic forces were screened out and local bonding considerations dominated the impurity state formation. The resulting defect states were referred to as deep defect states because they are formed by the central cell potential. Because the fundamental band gaps of IV–VI semiconductors are so small (∼0.2 eV), most of these perturbed energy levels could lie anywhere *vis-à-vis* the fundamental band gap.

For the sake of illustration let us consider Cs-row impurities at the Pb site. We start from pure PbTe with a Pb 'defect' at the Pb-site which has an s-level in the valence band and p-levels

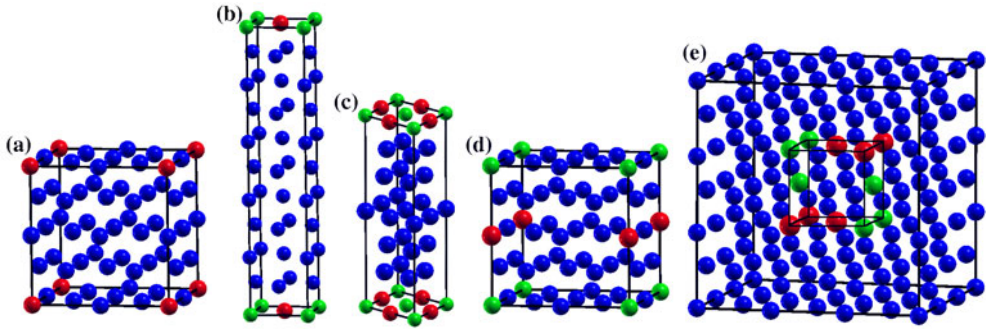

Figure 4. Unit cell models for (a) a single Ag impurity atom in $AgPb_{31}Te_{32}$, (b) a Ag–Sb layer perpendicular to the [001] direction in $AgSbPb_{18}Te_{20}$, (c) a Ag–Sb layer perpendicular to the fcc [111] direction in $AgSbPb_{10}Te_{12}$, (d) a Ag–Sb chain parallel to the [001] direction in $AgSbPb_{30}Te_{32}$ and (e) a Ag–Sb cluster in $AgSbPb_{16}Te_{18}$. For reasons of clarity we show only Pb fcc lattices with Pb in dark grey (blue), Ag in mid grey (red) and Sb in light grey (green).

in the conduction band. The conduction band is primarily Pb p-like and the Pb s states lie in the valence band. Making the defects more electropositive, i.e. going from column-IV to column-0, drives these defect levels up in energy until eventually the s-level crosses into the conduction band (between column-0 and column-I) to form the deep levels of the vacancy in the conduction band far above the CBM. Similarly making the defects more electronegative drives the energy levels down, so that the p-levels ultimately drop into the valence band. Lent *et al*'s calculations indicated that the defect p-levels cross the gap to the right of column-VIII. They showed that Bi (trivalent) impurity gave a resonant p-like state (more than 0.5 eV above the CBM) which was partially occupied. In contrast Cs impurities gave s-like deep defect states near the top of the valence band, which were partially occupied. In the next subsection we see how *ab initio* calculations that incorporate the screening effects properly, quantitatively justify some of these empirical findings.

3.2. Ab initio DFT calculations in $AgSbPb_{2n-2}Te_{2n}$

These compounds were originally designed to have an average cubic NaCl structure ($Fm\bar{3}m$ symmetry) with Ag, Pb and Sb atoms being statistically disordered on the Na sites. In fact powder x-ray diffraction studies support this model. However careful single crystal x-ray diffraction and electron diffraction studies reveal that is not the case [7]. There is clear experimental evidence that the Ag and Sb atoms are not statistically disordered with the Pb atoms. Instead there is a strong driving force that causes long range ordering in the crystal, the nature of which depends on the value of n and the exact experimental conditions with which the materials were prepared [7]. In fact it is possible to create a statistical disorder of all cations on the Pb sites in the samples (such as quenching from a melt) but such samples have inferior thermoelectric properties.

First, we performed calculations with isolated Ag and Sb impurity atoms in the PbTe lattice in order to obtain a clear picture of their individual role in modifying the electronic structure of PbTe (figure 4(a)). Then both Ag and Sb were introduced to simulate stoichiometries relevant to those of $AgSbPb_{2n-2}Te_{2n}$ compounds. Given that the exact crystal structure is not known, several plausible microstructural models were examined, all of which involved long range ordering of the atoms. In one model the Ag and Sb atoms were placed in monolayers (figures 4(b), (c)). In another model the Ag and Sb atoms were placed along straight infinite

chains running parallel to a crystallographic unit cell axis (e.g. c-axis) (figure 4(d)). In yet a third arrangement, the atoms were placed in the centre of a $3 \times 3 \times 3$ supercell to create a '$AgSbTe_2$ nanodot' embedded in a PbTe matrix (figure 4(e)). The chain and cluster models are in qualitative agreement with the experimental transmission electron microscopy (TEM) observations of Ag–Sb ordering [7]. Although we believe that these arrangements capture much of the crystal physics in these materials, we recognize that there are many more that could be considered which nevertheless should result in similar general conclusions.

To model the Ag (Sb) isolated and Ag–Sb pair impurities we have constructed $2 \times 2 \times 2$ supercells with 64 atoms. For the isolated case, we chose Ag (Sb) at the origin of the supercell with a separation of two lattice constants (12.924 Å) between the Ag (Sb) atoms (figure 4(a)). For the Ag–Sb pair, we considered two arrangements (not shown in figure 4), one where the Ag and Sb are far apart (Sb at the origin and Ag at the centre of the supercell) with a separation distance of ∼11.19 Å and the other where the Ag and Sb are as close as possible (Sb at the origin and Ag at the next nearest neighbour site of Sb) with a separation distance of ∼4.57 Å. For the structure where Ag–Sb layers are separated by several Pb layers we also considered two cases where the Ag–Sb layer is normal to the [001] direction in a $1 \times 1 \times 5$ supercell (40 atoms/cell) with the Ag–Sb layer located in the $z = 0$ plane (figure 4(b)) and where the Ag–Sb layer is normal to the [111] direction (figure 4(c)). The fcc unit cell can be viewed along the [111] direction as a hexagonal unit cell. We have used a $2 \times 2 \times 2$ hexagonal supercell (48 atoms/cell) with the Ag–Sb layer perpendicular to the c-axis which is the [111] direction in the fcc unit cell. To model the chains we used a $2 \times 2 \times 2$ supercell where the Ag–Sb chains are oriented parallel to the [001] direction (figure 4(d)) and separated by 12.924 Å. Finally, for the '$AgSbTe_2$' clusters we constructed a $3 \times 3 \times 3$ supercell (216 atoms/cell) and the cluster consists of six Ag–Sb pairs located at the centre of the supercell with a minimum separation distance between two clusters of ∼12.924 Å (figure 4(e)). Convergence of the self-consistent iterations was performed using 10 (for a single impurity and Ag–Sb pair impurities), 15 (for a layer of Ag–Sb pairs), 18 (for a chain of Ag–Sb pairs) and 2 (for a cluster of Ag–Sb pairs) k points inside the reduced Brillouin zones to within 0.0001 Ryd with a cutoff of -6.0 Ryd between the valence and the core states. For all calculations we use the experimental lattice constants of PbTe.

The total DOS for isolated Ag atoms is shown in figure 5(a). It can be seen that Ag introduces states near the top of the PbTe valence band (VB). Partial DOS analysis shows that these states consist mostly of p orbitals of the six nearest neighbour Te (Te2) atoms of Ag (figure 5(b)). These states are resonant with the VB and extend into the PbTe gap region. These observations confirm the existence of a deep defect level associated with Cs (monovalent impurity as Ag) in PbTe by Lent *et al* [14]. On the other hand the isolated Sb impurity introduces resonant states near the bottom of the PbTe conduction band (CB) (figure 5(c)) which extend nearly ∼0.75 eV into the CB starting from the CB bottom. Sb and its Te nearest neighbours (Te2) atoms have the highest contribution to these resonant states (figure 5(d)). The Sb p states hybridize with Te p states in the range $(-0.25, 2.5)$ eV. Therefore these states are not only resonant with the PbTe CB but they extend into the PbTe gap. A Bader analysis of the electronic charge for the Ag single impurity shows ionic states of $Ag^{+0.23}$ and $Te2^{-0.56}$, whereas for an Sb single impurity ionic states of $Sb^{+0.47}$ and $Te2^{-0.58}$ are found. These ionic states are very different from those assumed in the pure ionic model (Ag^{1+}, Sb^{3+} and Te^{2-}) suggesting a strong covalent interaction between Sb and Te atoms. We also have plotted the valence electronic charge density in the $(-1, 0.25)$ eV energy range for the Ag single impurity, bulk PbTe and the difference between these two electronic charge densities (figures 6(a)–(c)). Similarly for the Sb single impurity we have plotted the conduction charge density in the $(-0.5, 2)$ eV energy range in comparison with the conduction charge density

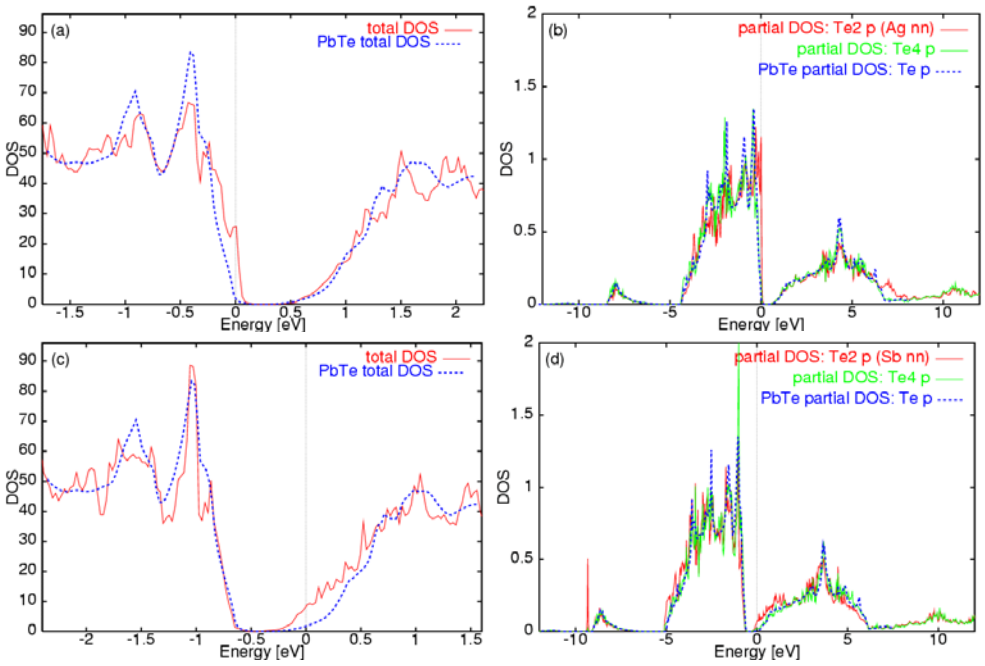

Figure 5. Total DOS of (a) a Ag and (c) an Sb single impurity atom in PbTe. For comparison the total DOS of bulk PbTe is shown as a dashed curve; (b) Partial p DOS of Te2 (Ag nearest neighbour), Te4 (away from Ag impurity), and Te in bulk PbTe; (d) Partial p DOS of Te2 (Sb nearest neighbour), Te4 (away from Sb impurity), and Te in bulk PbTe.

of bulk PbTe and the difference between these conduction charge densities (figures 6(d)–(f)). The charge density plots clearly show that the valence (conduction) electronic charge density associated with the Ag (Sb) single impurity is mostly localized on the Ag (Sb) impurity atom and its nearest neighbour Te atoms, consistent with the picture that these are deep defect levels. Both the VB states in the $(-1, 0.25)$ eV energy range and CB states in the $(-0.5, 2)$ eV energy range are antibonding states.

Results for isolated Ag–Sb pairs are consistent with the Ag (Sb) single impurity results in the sense that Ag introduces new states near the top of VB, whereas Sb introduces new states near the bottom of CB (figure 7) decreasing the PbTe gap. Both cases (Ag–Sb far apart and Ag–Sb next nearest neighbours) (not shown in figure 4) show semiconducting behaviour with a very small gap and a more rapidly increasing DOS near the VB and CB extrema as compared to the DOS of PbTe. The specific features of the DOS in the gap region are very different for these two cases. Total energy comparison for $AgSbPb_{30}Te_{32}$ shows that these two structures are very close in energy, the case when Ag–Sb atoms are far apart has a lower energy by $\sim$20 meV/(unit cell).

It is interesting to compare the DOS results for different layer structures of Ag–Sb (figures 4(b), (c)). When the Ag–Sb layer is perpendicular to the [001] direction, the states associated with the Ag–Sb layer completely fill the PbTe gap giving a semimetallic behaviour (figure 8(a)), whereas the Ag–Sb layer perpendicular to the [111] direction shows a semiconducting behaviour (figure 8(b)). This indicates that the electronic structure of $AgSbPb_{2n-2}Te_{2n}$ systems and consequently the electronic properties are very sensitive to the microstructures. The Ag–Sb chain model shows semiconducting behaviour (figure 8(c)).

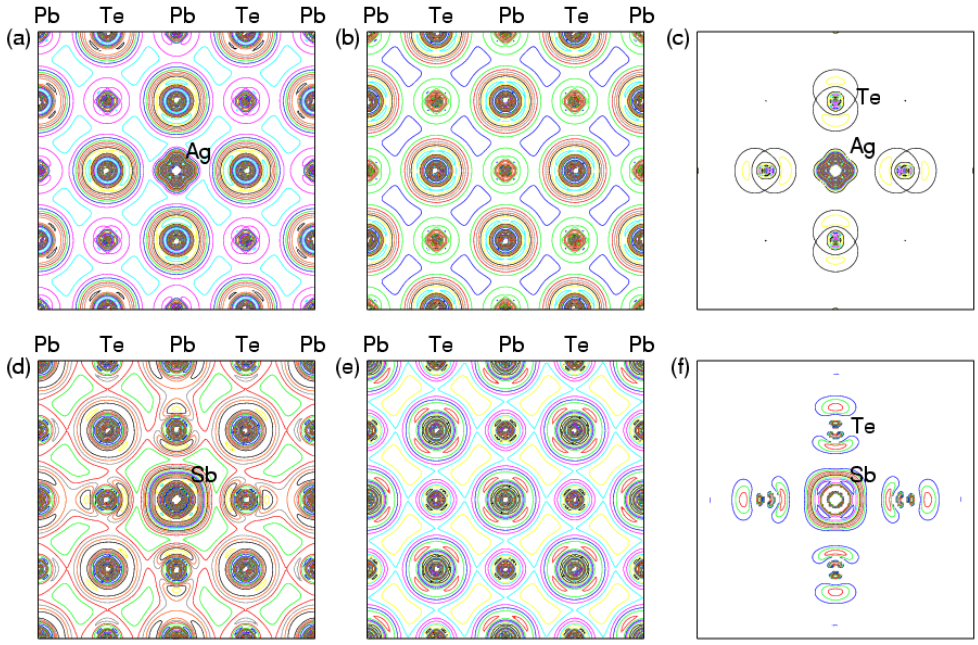

Figure 6. VB electronic charge density plots in plane perpendicular to the [001] direction in the $(-1, 0.25)$ eV energy range for (a) a Ag single impurity, (b) a bulk PbTe, and (c) the difference between a Ag single impurity and bulk PbTe. CB electronic charge density plots in plane perpendicular to the [001] direction in the $(-0.5, 2)$ eV energy range for (e) an Sb single impurity, (b) bulk PbTe, and (c) the difference between an Sb single impurity and bulk PbTe. The charge density is represented by closed lines from low charge density regions (electrons Å^{-3}) to high charge density regions (0.5 electrons Å^{-3}) in steps of 0.01 electrons Å^{-3}.

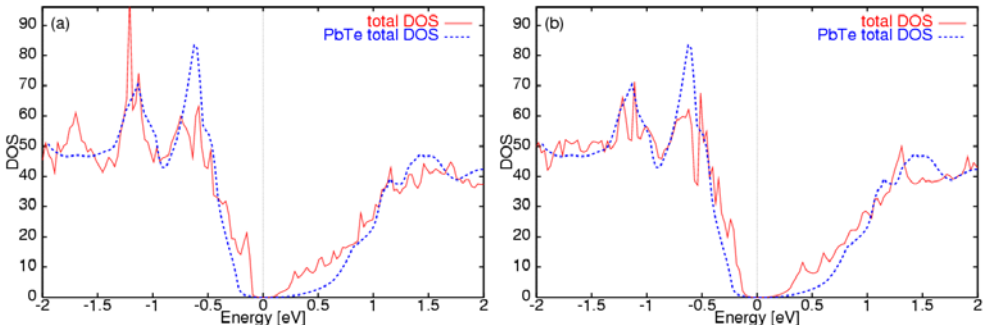

Figure 7. Total DOS of (a) a Ag–Sb pair impurity with the Ag–Sb distance of ∼11.19 Å, and (b) a Ag–Sb pair impurity with a Ag–Sb distance of ∼4.57 Å, in PbTe. For comparison the total DOS of bulk PbTe is shown as a dashed line.

This chain model has the same stoichiometry ($AgSbPb_{30}Te_{32}$) as the Ag–Sb pair impurity models. Total energy comparisons show that the chain model has a lower energy by 0.2 eV/(unit cell) than the Ag–Sb pair impurity models suggesting that Ag–Sb chain orderings along the [001] directions are favourable microstructures. This is consistent with the results of electron crystallographic studies which indicate the presence of Ag–Sb chains in the crystal [7]. The DOS results for the '$AgSbTe_2$' cluster model show also semiconductor behaviour (figure 8(d)).

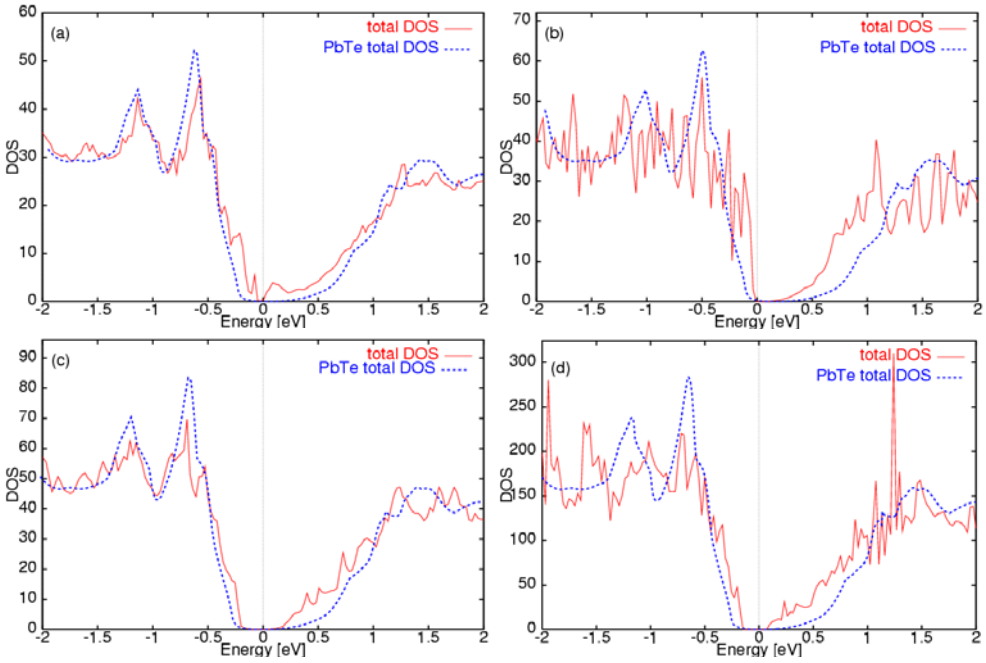

Figure 8. Total DOS of (a) a Ag–Sb layer model perpendicular to the [001] direction, (b) a Ag–Sb layer model perpendicular to the [111] direction, (c) a Ag–Sb chain model, and (d) a Ag–Sb cluster model. The total DOS of bulk PbTe is shown as a dashed curve.

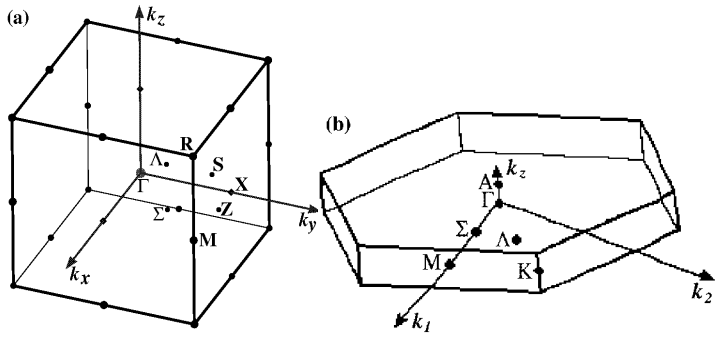

Figure 9. (a) Simple cubic Brillouin zone, (b) hexagonal Brillouin zone.

It is interesting to see how the PbTe band structure is affected by the microstructural arrangements of Ag–Sb pair impurities. To see the differences we plotted also the PbTe band structure in the simple cubic (sc) Brillouin zone given in figure 9(a). The band structures for bulk PbTe, a Ag–Sb chain model, a Ag–Sb pair impurity with a Ag–Sb distance of ∼11.19 Å, and a Ag–Sb layer model perpendicular to the [111] direction are shown in figure 10. In the sc Brillouin zone the CBM and VBM of bulk PbTe occur at the Γ point which is the same as the L point in the fcc Brillouin zone. For a Ag–Sb chain model and a Ag–Sb pair impurity with a Ag–Sb distance of ∼11.19 Å the CBM and VBM occur at the Γ point. For a Ag–Sb layer model perpendicular to the [111] direction, the CBM occurs at the Γ point, while the VBM occurs along the ΓK direction giving an indirect narrow band-gap semiconductor.

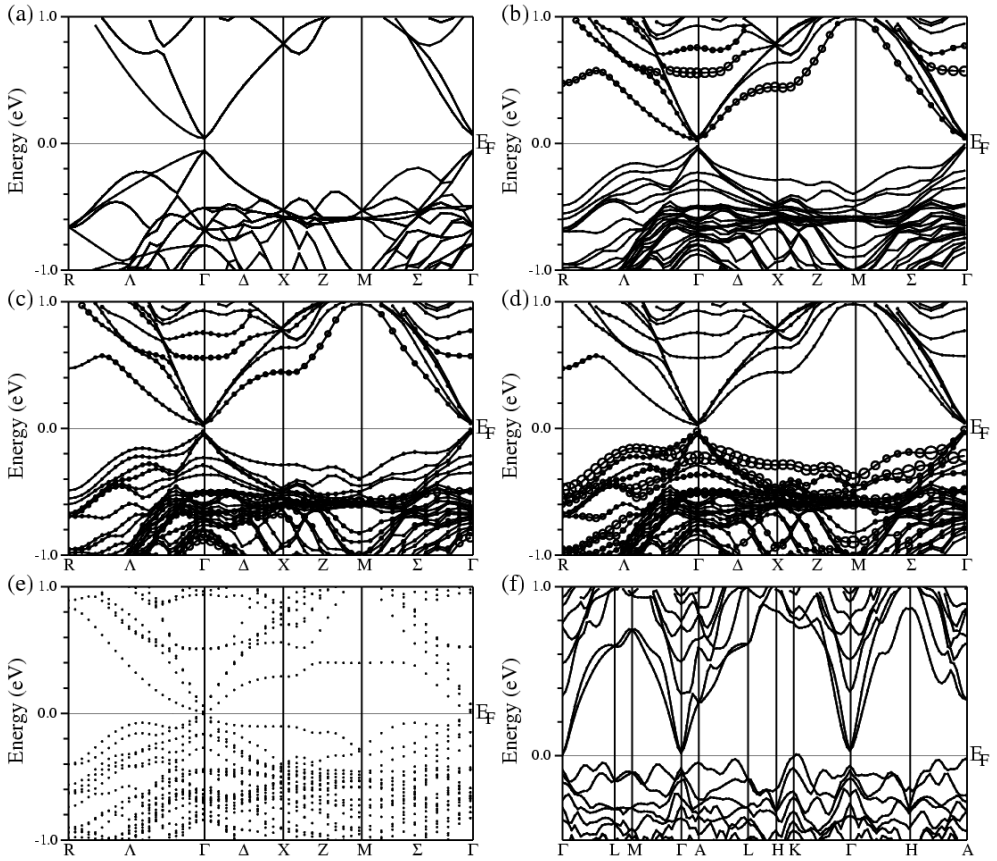

Figure 10. Band structure in the simple cubic Brillouin zone of (a) bulk PbTe, (b)–(d) Ag–Sb chain model; orbital character of (b) Sb p, (c) Te5 p (Sb nearest neighbour), and (d) Te6 p (Ag nearest neighbour), (e) Ag–Sb pair impurity with a Ag–Sb distance of ∼11.19 Å. Band structure in the hexagonal Brillouin zone of (f) Ag–Sb layer model perpendicular to the [111] direction.

4. Summary and conclusion

Our *ab initio* electronic structure calculations give a clear picture of the deep defect states in PbTe when nominally divalent Pb ion is substituted by Ag (monovalent) and Sb (trivalent) ions. Calculations for isolated Ag and Sb impurities and different microstructural arrangements of Ag–Sb show a generic feature; when Sb atoms replace Pb atoms, Sb hybridize with Te atoms forming strong covalent interactions. When Ag replaces Pb, the p states of Te, which are the nearest neighbours of Ag, are strongly perturbed. Therefore the electronic structure of $AgSbPb_{2n-2}Te_{2n}$ compounds depend sensitively on these Te states perturbed by the Ag (Sb) atoms. These deep defect states appear near the top of the valence band (for monovalent Ag) and overlap with the PbTe conduction band (for trivalent Sb). In the latter case they are clearly resonant states.

We have shown that the details of the DOS near the energy gap of $AgSbPb_{2n-2}Te_{2n}$ depend sensitively on the microstructural ordering arrangements of Ag–Sb pairs in PbTe. The nature of the states near the top VB and bottom CB in these quaternary compounds is substantially different than in PbTe. The common feature of these Ag–Sb arrangements is that they have a

more rapidly increasing DOS near the gap as compared to bulk PbTe due to the appearance of distinct resonant states. It is well accepted that resonant structures in the DOS near Fermi energy, created by quantum size effects [25, 26], superlattice engineering [27] or chemical means [28, 29] are very desirable features because they could enhance the thermoelectric figure of merit ZT.

Acknowledgments

We would like to thank Professor M G Kanatzidis and Dr K F Hsu for many helpful discussions. Financial support from the Office of Naval Research (Grant No. N00014-02-1-0867 MURI program) is acknowledged.

Note added in proof. Part of this work along with some experimental results will be published in Physical Review Letters (2004) **93** 146403.

References

[1] Agrawal G P and Dutta N K 1993 *Semiconductor Lasers* (New York: Van Nostrand-Reinhold) p 547
Chatterjee S and Pal U 1993 *Opt. Eng.* **32** 2923
[2] Chaudhuri T K 1992 *Int. J. Energy Res.* **16** 481
[3] Dughaish J H 2002 *Physica* B **322** 205
[4] Ioffe A F 1957 *Semiconductor Thermoelements and Thermoelectric Cooling* (London: Infosearch)
[5] Skrabek E A and Trimmer D S 1995 *CRC Handbook of Thermoelectrics* ed D M Rowe (Boca Raton, FL: CRC Press) p 267
[6] Harman T C, Spears D L and Manfra M J 1996 *J. Electron. Mater.* **25** 1121
Harman T C, Taylor P J, Walsh M P and LaForge B E 2002 *Science* **297** 2229
[7] Hsu K F, Loo S, Guo F, Chen W, Dyck J S, Uher C, Hogan T, Polychroniadis E K and Kanatzidis M G 2004 *Science* **303** 818
Quarez E, Hsu K F, Pcionek R and Kanatzidis M G 2004 in preparation
[8] Blake N P and Metiu H 2003 *Chemistry, Physics, and Materials Science of Thermoelectric Materials Beyond Bismuth Telluride* ed M G Kanatzidis, S D Mahanti and T Hogan (New York: Kluwer–Academic) p 259
[9] Mahanti S D, Larson P M, Bilc D and Li H 2003 *Chemistry, Physics, and Materials Science of Thermoelectric Materials Beyond Bismuth Telluride* ed M G Kanatzidis, S D Mahanti and T Hogan (New York: Kluwer–Academic) p 227
[10] Nolas G S, Sharp J and Goldsmidt H J 2001 *Thermoelectrics Basic Principles and New Materials Development* (Berlin: Springer)
[11] Pantelides S T 1992 *Deep Centers in Semiconductors* 2nd edn (Yverdon, Switzerland: Gordon and Breach)
[12] Kohn W 1957 *Solid State Physics* vol 5, ed F Seitz and D Turnbull (New York: Academic) chapter 4
[13] Panteledis S T 1978 *Rev. Mod. Phys.* **50** 797
[14] Lent C S, Bowen M A, Dow J D, Allgaiger R S, Sankey O F and Ho E S 1987 *Solid State Commun.* **61** 83
[15] Conkin J B, Johnson L E and Pratt G W 1965 *Phys. Rev.* **137** A1282
Lin P J and Kleinmann L 1966 *Phys. Rev.* **142** 478
Rabii S 1968 *Phys. Rev.* **167** 801
Herman F, Kortum R L, Ortenburger I and Van Dyke J P 1968 *J. Physique* **29** (Suppl.) C4 62
Tang Y W and Cohen M L 1969 *Phys. Rev.* **180** 823
Buss D D and Parade N J 1970 *Phys. Rev.* B **1** 2692
Kohn S E, Yy P Y, Petroff Y, Shen Y R, Tsang Y and Cohen M L 1973 *Phys. Rev.* B **8** 1477
Martinez G, Schluter M and Cohen M L 1975 *Phys. Rev.* B **11** 651
Nimtz G and Schlicht B 1983 *Narrow-Gap Semiconductors* (Berlin: Springer) p 35
Lent C S, Bowen M A, Dow J D, Allgaiger R S, Sankey O F and Ho E S 1986 *Superlatt. Microstruct.* **2** 491
Wei S H and Zunger A 1997 *Phys. Rev.* B **55** 13605
Delin A, Ravindran P, Eriksson O and Wills J M 1998 *Int. J. Quantum Chem.* **69** 349
Lach-hab M, Keegan M, Papaconstantopoulos D A and Mehl M J 2000 *J. Phys. Chem. Solids* **61** 1639
Albanesi E A, Okoye C M I, Rodriguez C O, Peltzer y Blanca E L and Petukhov A G 2000 *Phys. Rev.* B **61** 16589

[16] Wei S W and Zunger A 1997 *Phys. Rev.* B **55** 13605
[17] Hohenberg P and Kohn W 1964 *Phys. Rev.* **136** B864
Kohn W and Sham L 1965 *Phys. Rev.* **140** A1133
[18] Singh D J 1994 *Planewaves, Pseudopotentials, and the LAPW Method* (Boston, MA: Kluwer–Academic)
[19] Albanesi E A, Okoye C M I, Rodriguez C O, Peltzer y Blanca E L and Petukhov A G 2000 *Phys. Rev.* B **61** 16589
[20] Perdew J P, Burke K and Ernzerhof M 1996 *Phys. Rev. Lett.* **77** 3865
[21] Blaha P *et al* 2001 *WIEN2K, An Augmented Plane Wave + Local Orbitals Program for Calculating Crystal Properties* ed K Schwarz (Techn. Universitat Wien, Austria)
[22] Koelling D D and Harmon B 1980 *J. Phys. C: Solid State Phys.* **13** 6147
[23] Bader R F W 1990 *Atoms in Molecules—A Quantum Theory* (Oxford: Oxford University Press)
[24] Dronskowski R and Blochl P E 1993 *J. Phys. Chem.* **97** 8617
[25] Hicks L D and Dresselhaus M S 1993 *Phys. Rev.* B **47** 12727
[26] Harman T C, Taylor P J, Walsh M P and LaForge B E 2002 *Science* **297** 2229
Hicks L D, Harman T C and Dresselhaus M S 1993 *Appl. Phys. Lett.* **63** 3230
[27] Venkatasubramanian R, Siivola E, Colpitts T and O'Quinn B 2001 *Nature* **413** 597
[28] Mahan G D and Sofo J O 1996 *Proc. Natl Acad. Sci.* **93** 7436
[29] Kanatzidis M G 2001 *Semicond. Semimet.* **69** 51
Kanatzidis M G 2003 *Chemistry, Physics, and Material Science of Thermoelectric Materials: Beyond Bismuth Telluride* ed M G Kanatzidis, S D Mahanti and T Hogan (New York: Kluwer–Academic) p 35